Host genetic control of natural killer cell diversity revealed in the Collaborative Cross

Magali S. J. Dupont[a,b,c], Vincent Guillemot[d], Pascal Campagne[d], Nicolas Serafini[a,b], Solenne Marie[a,b], Xavier Montagutelli[e], James P. Di Santo[a,b], and Christian A. J. Vosshenrich[a,b,1]

[a]Innate Immunity Unit, Immunology Department, Institut Pasteur, 75724 Paris, France; [b]INSERM U1223, 75724 Paris, France; [c]Université de Paris, Sorbonne Paris Cité, 75013 Paris, France; [d]Bioinformatics and Biostatistics Hub, Computational Biology Department, Institut Pasteur, 75724 Paris, France; and [e]Mouse Genetics Laboratory, Department of Genomes and Genetics, Institut Pasteur, 75724 Paris, France

Edited by Lewis L. Lanier, University of California San Francisco Medical Center, San Francisco, CA, and approved January 8, 2021 (received for review September 10, 2020)

Natural killer (NK) cells are innate effectors armed with cytotoxic and cytokine-secreting capacities whose spontaneous antitumor activity is key to numerous immunotherapeutic strategies. However, current mouse models fail to mirror the extensive immune system variation that exists in the human population which may impact on NK cell-based therapies. We performed a comprehensive profiling of NK cells in the Collaborative Cross (CC), a collection of novel recombinant inbred mouse strains whose genetic diversity matches that of humans, thereby providing a unique and highly diverse small animal model for the study of immune variation. We demonstrate that NK cells from CC strains displayed a breadth of phenotypic and functional variation reminiscent of that reported for humans with regards to cell numbers, key marker expression, and functional capacities. We took advantage of the vast genetic diversity of the CC and identified nine genomic loci through quantitative trait locus mapping driving these phenotypic variations. SNP haplotype patterns and variant effect analyses identified candidate genes associated with lung NK cell numbers, frequencies of CD94$^+$ NK cells, and expression levels of NKp46. Thus, we demonstrate that the CC represents an outstanding resource to study NK cell diversity and its regulation by host genetics.

NK cells | innate immunity | Collaborative Cross | quantitative trait locus mapping

Natural killer (NK) cells are innate cytotoxic lymphoid cells lacking rearranged antigen-specific receptors (1). Upon recognition of infected, cancerous, or stressed cells, NK cells can rapidly exert cytolytic activity through granule- and/or cell-surface death ligand–mediated mechanisms; they also secrete high concentrations of cytokines IFN-γ and tumor necrosis factor that activate proinflammatory circuits (2, 3). The innate reactivity of NK cells is crucial for cancer immunosurveillance and for dictating the early immune response to viral or intracellular bacterial infections (4, 5). NK cell–based approaches are being exploited in increasing numbers for cancer immunotherapies (https://clinicaltrials.gov/, search term: NK cells and NK cell therapy).

Both mouse and human NK cells consist of heterogeneous subsets that are phenotypically and functionally distinct (6). Analyses of inbred mouse strains including 129S1/SvlmJ, BALB/c, and principally C57BL/6 have led to fundamental discoveries in NK cell biology (7–10). Nonetheless, inbred mice are unable to model the wide range of immune phenotypes observed in the human population under homeostasis or inflammatory conditions as their genetic diversity is much more limited compared to that of humans (11, 12). One example is CD94 that forms heterodimers with NKG2 family members, including NKG2A or C, exhibiting inhibiting or activating functions depending on the partner subunit (13). It is expressed at stable frequencies of around 50% by NK cells from C57BL/6J (B6) and other inbred strains like 129S1/SvlmJ (14), which contrasts with the wide range of frequencies of CD94$^+$ NK cells observed in humans (12). Similarly, NK cell numbers vary little in inbred strains, while in humans, extensive interindividual variation has been reported (11, 15).

Novel mouse resources have been generated that harbor genetic diversity matching that of humans. One such model is the Collaborative Cross (CC), a genetically diverse mouse-mapping population designed by the Complex Trait Consortium (16). The CC represents a panel of recombinant inbred strains derived from the intercrossing of five common laboratory strains and three wild-derived strains representing the three main *Mus musculus* subspecies (*M.m. domesticus*, *M.m. musculus*, and *M.m. castaneus*). Together, the CC strains harbor 45 million segregating polymorphisms and capture 90% of the genetic diversity present in the *M. musculus* species (16). This far exceeds the 4 million polymorphisms present in most classical inbred strains (17, 18). CC strains have been shown to display broad variation of immune parameters (19–21), and studies using CC mice have led to the identification of novel genes associated with susceptibility to pathogens like *Salmonella* Typhimurium (22) or West Nile Virus (23) and of novel mouse models for human infectious diseases (24–26). This demonstrates that the CC is a powerful model to explore the molecular mechanisms underlying immune variation.

We took advantage of the CC resource to characterize NK cell phenotypic and functional diversity. Based on our analysis of more than 220 mice across 32 CC strains, we observed an extensive variation in absolute NK cell numbers, differentiation states, key marker expression, and functional capacities in vitro. By exploiting the genetic diversity of the CC, we identified nine quantitative

Significance

Our work reveals the breadth of NK cell immune variation present in the *Mus musculus* species as represented by the highly diverse Collaborative Cross (CC) mouse resource. We identify unique CC strains that provide an opportunity to study NK cell differentiation and function, and we identify genomic loci driving the variation of relevant NK cell parameters including lung NK cell numbers, frequencies of CD94$^+$ NK cells, and expression levels of NKp46. Finally, our results reveal the similarities of NK cell immune variation between genetically highly diverse human and mouse populations, highlighting the potential of CC mice as a preclinical model for the development of immunotherapies targeting NK cells.

Author contributions: X.M., J.P.D.S., and C.A.J.V. designed research; M.S.J.D., N.S., S.M., and C.A.J.V. performed research; M.S.J.D., V.G., P.C., X.M., and C.A.J.V. analyzed data; and M.S.J.D. and C.A.J.V. wrote the paper.

The authors declare no competing interest.

This article is a PNAS Direct Submission.

[1]To whom correspondence may be addressed. Email: christian.vosshenrich@pasteur.fr.

This article contains supporting information online at https://www.pnas.org/lookup/suppl/doi:10.1073/pnas.2018834118/-/DCSupplemental.

Published March 1, 2021.

trait loci (QTL) that drive variations in unique parameters of NK cell biology.

Results

Extensive Variation of NK Cell Numbers in the CC. We assessed the phenotypic diversity of NK cells at homeostasis in adult mice in four different organs from 32 CC strains compared to control B6 mice. More specifically, we focused on the variation of NK cell numbers, differentiation stages as defined by CD27, CD11b, and KLRG1 expression patterns, and expression of other NK cell surface and intracellular markers, including CD94, DNAM-1, NKp46, and the transcriptions factors (TF) Eomesodermin (Eomes) and T-bet.

NK cells were identified through the combined expression of NKp46 that marks NK cells across species (27) and the TFs Eomes and T-bet, which are important regulators of NK cell development (*SI Appendix*, Fig. S1*A*) (28, 29). Total cell counts per organ varied among the CC strains (*SI Appendix*, Table S1). Absolute numbers as well as frequencies of splenic NK cells varied markedly between CC strains (Fig. 1*A* and *SI Appendix*, Fig. S1*B*); however, cell numbers and frequencies did not correlate. Average splenic NK cell numbers varied up to 25-fold ranging from 0.5×10^6 (CC037) to more than 12.5×10^6 (CC001; Fig. 1*A*). In comparison, B6 mice harbored on average 4×10^6 splenic NK cells (Fig. 1*A*). We observed a similar strong variation in absolute NK cell numbers and frequencies in lymphoid (mesenteric lymph nodes [mLN]) and nonlymphoid (liver and lung) organs of the same mice (Fig. 1*B* and *SI Appendix*, Fig. S1*B*). Similarly, absolute cell numbers of adaptive lymphocytes, including $CD3^+$ $CD5^+$ T cells and $CD19^+$ B cells, varied as well, although to a lesser extent (*SI Appendix*, Fig. S1*C*). Variations in the absolute numbers of NK and T cells led to a remarkable range in the spleen of T-to-NK cell ratios among the CC strains, ranging from 65:1 (CC037) to 1.25:1 (CC028). As a comparison, B6 displayed a ratio of 10:1 (Fig. 1 *C* and *D*). Similar great ranges of the T-to-NK cell ratios were observed in all organs (Fig. 1 *C* and *D* and *SI Appendix*, Fig. S2). Of note, some CC strains harbored similar or even higher NK than T cell numbers in liver (CC041, CC042, and CC075) and/or lung (CC007, CC009, CC013, CC027, CC028, CC041, and CC042) (Fig. 1*D* and *SI Appendix*, Fig. S2). For example, CC043 mice harbored three times more NK cells than T cells in the lung and CC042 mice 2.3 times more NK cells than T cells in the liver (Fig. 1*D* and *SI Appendix*, Fig. S2). However, T cells always prevailed in the spleen and mLN (Fig. 1 *C* and *D* and *SI Appendix*, Fig. S2). NK cell numbers correlated between spleen, liver, and lung (Fig. 1 *E* and *F*; Pearson's $R > 0.5$), which appeared coherent with their recirculation capacity. We did not observe any correlation between NK and T or B cell numbers in those same organs (Fig. 1*E*; Pearson's $R < 0.5$). In contrast, the numbers of NK cells and adaptive lymphocytes were strikingly correlated in mLN (Pearson's $R \geq 0.70$), thus suggesting a common factor driving NK, T, and B cell counts at this site (Fig. 1 *E* and *G*).

NK Cells from CC Mice Display Diverse Patterns of Cellular Differentiation. NK cell differentiation in peripheral lymphoid and nonlymphoid tissues can be delineated through specific expression patterns of CD27 and CD11b (30–32). The least differentiated NK cells express neither molecule (double negative [DN]) and sequentially gain CD27 (CD27 single positive [CD27SP]) followed by CD11b expression (double positive [DP]) before downregulating CD27 (CD11bSP) (30). In adult B6 mice, the frequency of DN NK cells was very low in the spleen (around 5%, Fig. 2*A* and *SI Appendix*, Fig. S3*A*). CD27SP and DP subsets represented around 10 and 20%, respectively, while the mature CD11bSP population was the major subset, accounting for 60 to 70% of total splenic NK cells (Fig. 2*A* and *SI Appendix*, Fig. S3 *B–D*). In most CC strains, DN and DP NK cells were minor subsets (2 to 25%) (Fig. 2*A* and *SI Appendix*, Fig. S3 *A* and *C*). In contrast, the proportion of CD27SP cells varied considerably: in CC001, this subset was marginal (2 to 4%), while it represented the largest subset in strains CC003, CC061, and CC075, accounting for up to 50% of total splenic NK cells (Fig. 2*A* and *SI Appendix*, Fig. S3*B*). Likewise, the proportion of CD11bSP was highly variable, ranging from 85% in CC001 to 25% in CC003 (Fig. 2*A* and *SI Appendix*, Fig. S3*D*).

The cadherin receptor KLRG1 is co-expressed with CD11b and thought to mark terminally differentiated NK cells (32–34). However, given the inhibitory activity of KLRG1, it was also suggested that it might be a marker of NK cell senescence or exhaustion (33–35). Around 40% of all splenic NK cells expressed KLRG1 in B6, while this proportion ranged from 10% (CC075) to more than 80% (CC013) across CC strains (Fig. 2*B*). Considering the inhibitory properties of KLRG1, such variations, observed both in spleen and liver (Fig. 2*B*), potentially impact functional capacities of NK cells. Moreover, the frequencies of $KLRG1^+$ NK cells were positively correlated with CD11bSP (Fig. 2*C*) but negatively with DP (*SI Appendix*, Fig. S3*E*) or CD27SP across the CC strains (Fig. 2*C*). This suggests that, although proportions of mature NK cell subsets were variable, KLRG1 expression was similarly regulated in most CC strains and B6.

NK Cells Display a High Phenotypic Diversity in the CC. We further assessed phenotypic NK cell variation through analysis of key surface and intracellular marker expression as mentioned above. CD94 associates with NKG2 family members, forming activating receptors with NKG2C and NKG2E and inhibitory receptors with NKG2A. Previous studies identified CD94 as a marker of more functional NK cells (36) and in humans of memory-like NK cells in the context of HIV infection (37). In B6, the proportion of $CD94^+$ NK cells varies with age, as almost all fetal or newborn NK cells express this protein (38, 39), while this frequency decreases to and remains at around 50% in adult mice (Fig. 3 *A* and *B*) (38). We observed a large and continuous variation of the frequency of $CD94^+$ splenic NK cells across the CC strains (Fig. 3 *A* and *B*). Most CC strains harbored between 30 and 60% $CD94^+$ splenic NK cells. The strains CC075 and CC043 presented the most extreme profiles, with respectively around 10% and 80% of $CD94^+$ NK cells resulting in an almost sevenfold difference between these strains (Fig. 3 *A* and *B*). Expression of CD94 did not correlate with CD27, CD11b, or KLRG1 indicating that CD94 expression was not associated to NK cell differentiation.

DNAM-1 is an activating receptor with an essential role in NK cell–mediated tumor surveillance (40) and NK cell memory formation and maintenance upon murine cytomegalovirus infection (41). More recently it has also been identified as a marker of NK cells with increased functional potential (42). As for CD94 expression, we observed a continuous variation of the frequencies of DNAM-1^+ NK cells in the spleen and mLN across our panel of CC strains (Fig. 3 *A* and *B*). In the spleen, this variation ranged from 25% for CC039 to 85% for CC013, and in the mLN, it ranged from 35% for CC061 to more than 90% for CC028. Moreover, while around 50% of B6 NK cells express DNAM-1 in both organs, we observed that a majority of the CC strains were displaying a much larger DNAM-1^+ NK population (Fig. 3 *A* and *B*). DNAM-1 expression by splenic NK cells was neither correlated to the expression of the differentiation markers nor CD94 (*SI Appendix*, Fig. S4*A*).

NKp46 is an evolutionarily conserved activating receptor that can identify NK cells across multiple species with important roles in immune responses to several types of infections including influenza or meningococcal infections as well as cancers (43). Interestingly, we found that NKp46 expression levels were not continuously distributed among CC strains. Rather, two groups of mice emerged based on NKp46 expression levels: one group expressing levels similar to B6 and a second group expressing around two- to threefold higher levels (colored boxes, Fig. 3 *C* and *D*). NKp46 expression levels were highly correlated across NK cells from the different organs (Fig. 3*E* and *SI Appendix*, Fig. S4*B*).

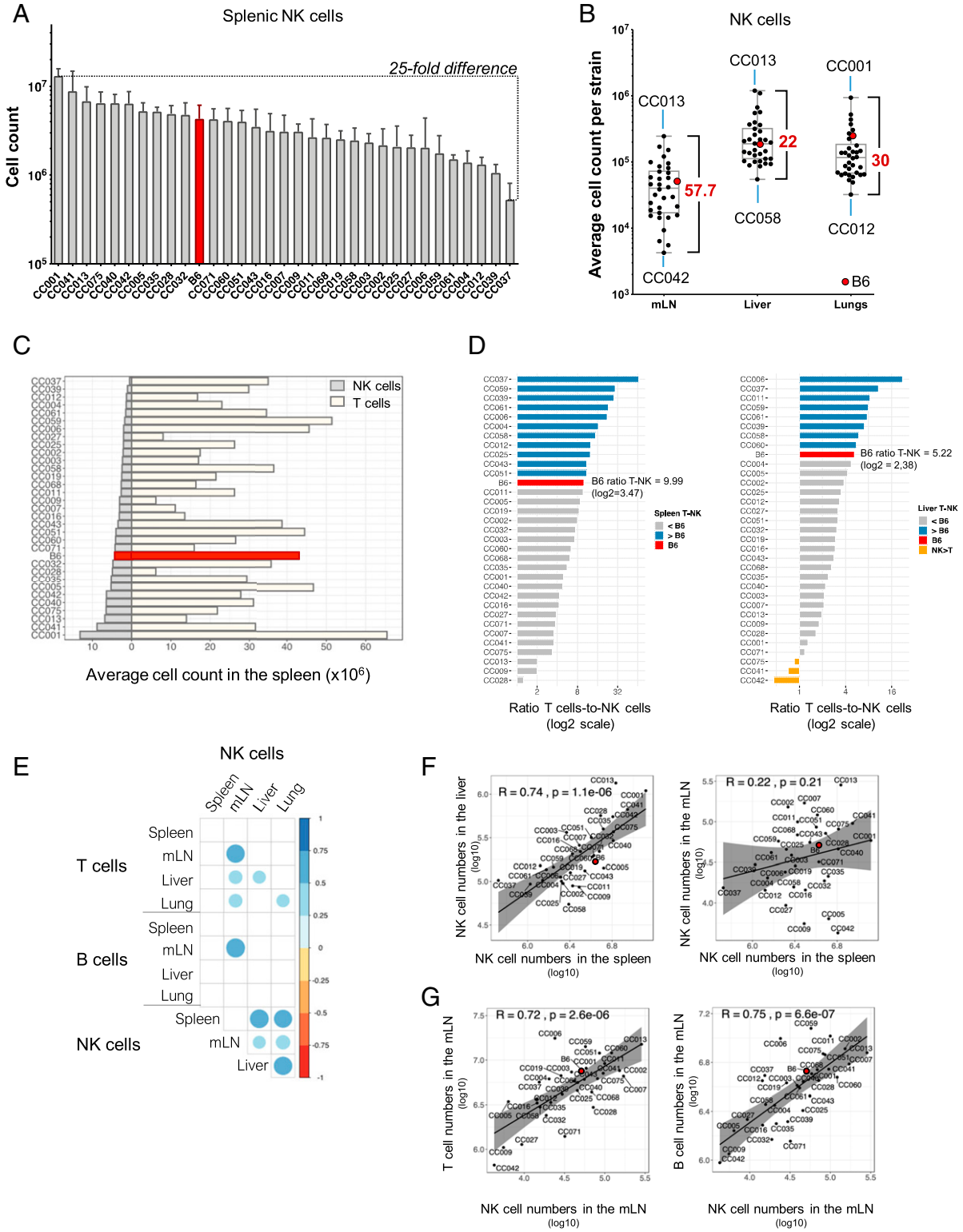

Fig. 1. Extensive variation of NK cell numbers in the CC strains. (*A*) Absolute number of splenic NK cells was determined by flow cytometry in the indicated strains. Data are represented as mean ± SD (*B*) Average NK cell numbers in the mLN, liver, and lung. The fold difference between the two extreme strains is highlighted in red, and each dot represents the average value of one CC strain. (*C*) Pyramid plot of the average splenic NK and T cell numbers in the indicated strains. (*D*) Ratio of T cells to NK cells in the spleen (*Left*) and liver (*Right*) in the indicated strains (log2 scale). (*E*) Correlation plot (Pearson) of the average NK, T, and B cell numbers in the spleen, mLN, liver, and lung across all CC strains. Nonsignificant correlations ($P > 0.05$) are blank. (*F*) Correlation graphs of the average numbers of splenic against hepatic NK cells (*Left*), splenic NK cells, and NK cells in the mLN (*Right*). (*G*) Correlation graphs of the average numbers of NK cells against T cell (*Left*) and B cell (*Right*) numbers in the mLN across all the CC strains and B6. Regression lines, Pearson's R coefficients, and *P* values are shown on the graphs. Mean values for the CC strains were calculated with on average five mice per CC line (see *Experimental Procedures* for more details) and B6 with 27 to 29 mice.

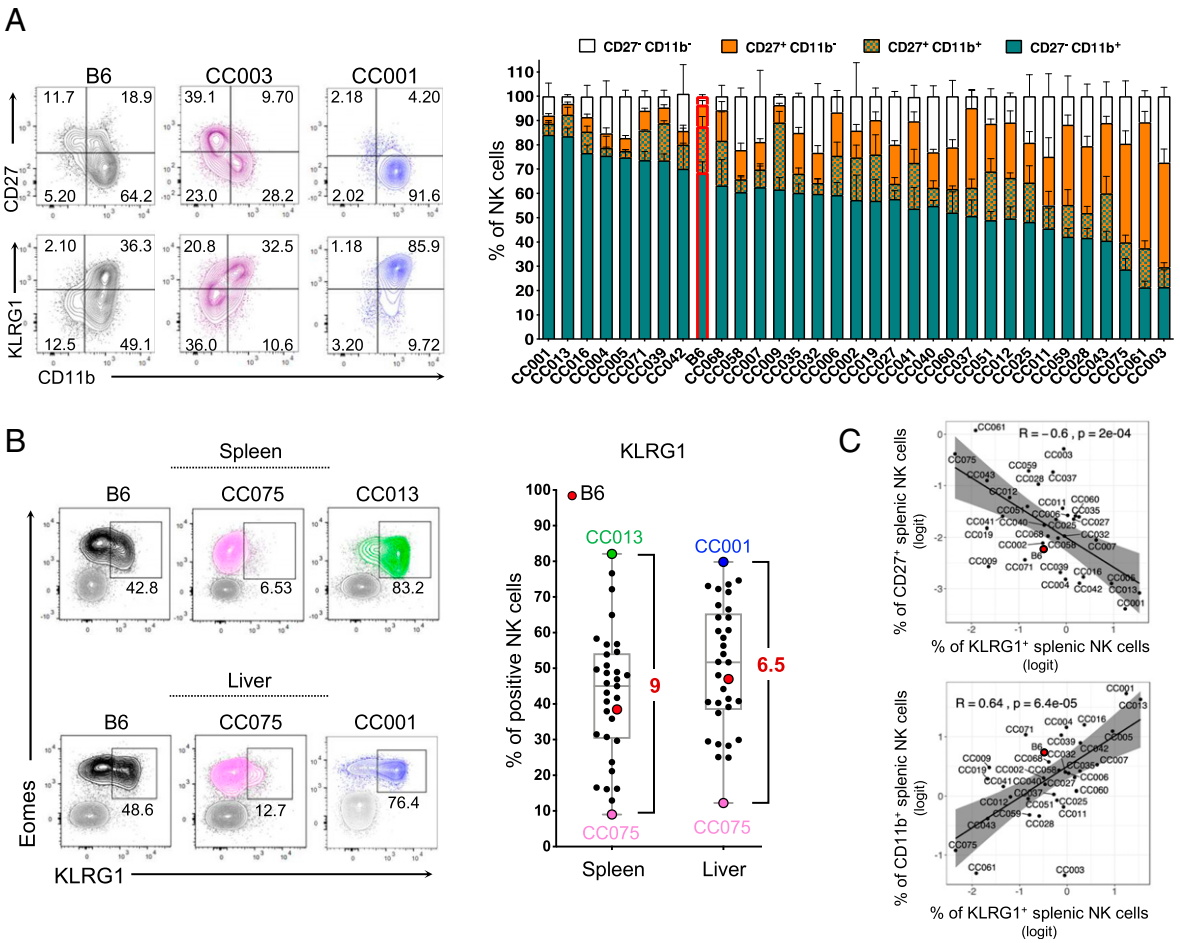

Fig. 2. NK cells present diverse patterns of cellular differentiation in the CC strains. (*A*, *Left*) Representative contour plots of the expression of CD27 versus CD11b (*Top*) and KLRG1 versus CD11b (*Bottom*) by splenic NK cell from B6, CC003, and CC001; (*Right*) bar graph summarizing percentages of $CD27^{-}CD11b^{-}$, $CD27^{+}CD11b^{-}$, $CD27^{+}CD11b^{+}$, and $CD27^{-}CD11b^{+}$ splenic NK cell subsets for the indicated strains. Data are represented as mean ± SD. (*B*, *Left*) Representative contour plots of Eomes versus KLRG1 expression by splenic and hepatic NK cells from B6, CC075, CC013, and CC001; (*Right*) average percentages of $KLRG1^{+}$ cells among NK cells in the spleen and liver of all CC strains and B6. The fold difference between the two extreme CC strains is given in red. The extreme strains are identified and color highlighted according to the colors in the contour plots on the *Left*. B6 is highlighted as a red dot. B cells (light gray) were used as negative population and overlaid on the contour plots. For (*A*) and (*B*), numbers on contour plots indicate the percentage of cells within the indicated gates. (*C*) Correlation graphs of the average percentage of $CD27^{+}$ (*Top*) and percentage of $CD11b^{+}$ (*Bottom*) against the percentage of $KLRG1^{+}$ splenic NK cells across all CC strains. Regression lines, Pearson's R coefficients, and *P* values are indicated. Mean values for the CC strains were calculated with on average five mice per CC line (see *Experimental Procedures* for more details) and B6 with 27 to 29 individuals.

Finally, when analyzing the expression levels of the TFs T-bet and Eomes, we noticed a more limited variation as most CC strains expressed them at 0.75 to 1.5-fold of B6 levels. However, some outlier strains like CC060 displayed more divergent T-bet expression levels (*SI Appendix*, Fig. S4 *C* and *E*). Moreover, expression of each TF also correlated between NK cells from the different tissues we analyzed (*SI Appendix*, Fig. S4 *D* and *F*).

NK Cells from the CC Strains Display Functional Variation In Vitro. One hallmark of NK cell functional responses is the secretion of cytokines, especially IFN-γ. For the functional analysis, we selected CC strains that presented unusual profiles for at least one of the previously described parameters: for instance, CC001 presented a highly mature/exhausted NK cell population as 90% of the splenic NK cells were CD11bSP and $KLRG1^{+}$. In contrast, CC061 harbored predominantly immature NK cells (CD27SP) in the spleen. NK cells from CC042 expressed high levels of NKp46, and CC037 presented the lowest splenic NK cell count. We assessed the capacity of NK cells from these strains to produce IFN-γ upon a 4-h stimulation with the inflammatory cytokines IL-12 and IL-18 or phorbol 12-myristate 13-acetate (PMA) and ionomycin. Both stimuli induced IFN-γ production by around 70% of B6 and CC059 NK cells (Fig. 4*A*). NK cells from two (CC001 and CC042) out of the seven tested CC strains produced significantly less IFN-γ under both conditions, while NK cells from CC019 and CC061 showed a reduction of IFN-γ production in response to IL-12 and IL-18 but not to PMA and ionomycin. In contrast, NK cells from CC002 mice displayed a specific reduction of IFN-γ production in response to PMA and ionomycin but not IL-12 and IL-18 stimulation (Fig. 4*A*).

A second functional hallmark of NK cells is the elimination of target cells through granule-mediated release of granzyme B and perforin. At steady-state and upon IL-2 stimulation, only CC059 NK cells contained significantly lower granzyme B levels while all other CC strains harbored amounts similar to those from B6 (*SI Appendix*, Fig. S5). Moreover, granzyme B expression was restricted to $CD11b^{+}$ NK cells in all strains (Fig. 4*B*). During a cytotoxic response, lytic granules containing granzyme B are released onto target cells, exposing at the same time the granule marker CD107a at the cell surface. We thus assessed the proportion of degranulating NK cells in the various CC strains by measuring CD107a surface expression upon stimulation. Around 20% of B6 NK cells degranulated in response to NKp46 stimulation in

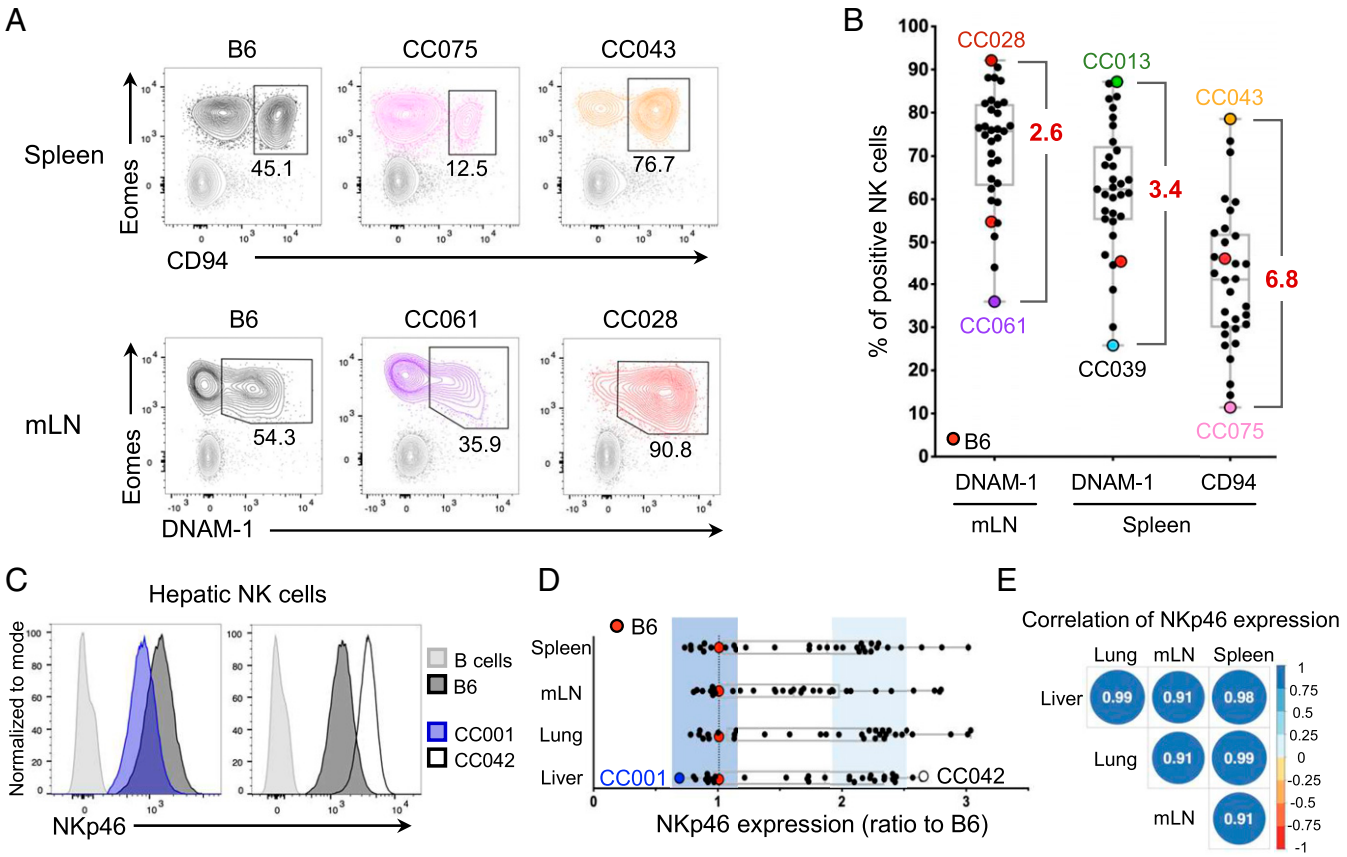

Fig. 3. NK cells display a high phenotypic variation in the CC strains. (*A*) Representative contour plots of Eomes versus CD94 expression (*Top*) by splenic NK cells in B6, CC075, and CC043 and expression of Eomes versus DNAM-1 (*Bottom*) by NK cells in the mLN in B6, CC061, and CC028. B cells (light gray) were used as negative population and overlaid on histograms. Numbers on contour plots indicate the percentage of cells within the indicated gates. (*B*) Average frequencies of NK cells expressing CD94 in spleen and DNAM-1 in mLN and spleen and of the indicated CC strains. The extreme CC strains are identified and color highlighted according to the colors in the contour plots in *A*. B6 is highlighted as a red dot. The fold difference between the two extreme strains is indicated in red. (*C*) Representative histogram overlays of NKp46 expression by hepatic NK cells from B6, CC001, and CC042. B cells (light gray) were used as negative population and overlaid on histograms. (*D*) Ratio of NKp46 expression in the spleen, mLN, lung, and liver of all CC strains and B6. The extreme strains are identified and color highlighted according to the colors in the contour plots in *C*. The colored boxes indicate two groups of mice expressing NKp46 at distinct levels in spleen, liver, and lung. Deep blue = expression levels are similar to that observed in B6 (ratio ~1); light blue = expression levels are two- to three-fold higher than in B6. B6 is highlighted as a red dot. (*E*) Correlation plots of average NKp46 expression in the liver, lung, mLN and spleen across all CC strains. Mean values for the CC strains were calculated with on average five mice per CC strain (see *Experimental Procedures* for more details) and B6 with 27 to 29 individuals.

presence of IL-2 in vitro (Fig. 4*C*). Similar results were obtained using NK cells from CC001, CC002, CC019, and CC037 (Fig. 4*C*), while significantly more NK cells from CC003, CC042, CC051, CC059, and CC061 mice degranulated under these conditions (Fig. 4 *C* and *D*). When considering the expression levels of NKp46 in relation to these results, we found that they were correlated to the degranulation capacity of NK cells (Fig. 4*D*; Pearson's R = 0.73). NK cells expressing low levels of NKp46 (B6, CC001, and CC019) had a reduced degranulation capacity compared to NK cells expressing high levels of NKp46 (CC003, CC042, CC051, and CC059; Fig. 4*D*). Noteworthy, strains CC002 and CC037 did not fit this model as their NK cells expressed intermediate levels of NKp46 and yet presented the same degranulation capacity as NK cells from B6, suggesting that they might be less responsive to NKp46 stimulation. Likewise, CC061 NK cells expressed low levels of NKp46 while degranulating twice as much as B6 NK cells indicating that CC061 NK cells might be more sensitive to stimulation via NKp46 (Fig. 4*D*). Of note, both CD11b$^+$ as well as CD11b$^-$ NK cells from CC061 mice degranulated upon stimulation via NKp46 and IL-2, while in B6 mice, this was restricted to CD11b$^+$ NK cells (Fig. 4*E*).

QTL Mapping of the CC Strains Uncovers Loci Controlling NK Cell Numbers and Phenotypes. Compiled results of the phenotypic analyses are presented in a heatmap with the rank of each CC strain for each parameter (*SI Appendix*, Fig. S6). This heatmap shows a very heterogeneous phenotype distribution with each CC strain displaying a distinctive pattern underscoring the extensive NK cell diversity present in the CC (*SI Appendix*, Fig. S6).

We sought to identify the impact of host genetics on the observed immune variations. Indeed, broad-sense heritability analyses returned scores higher than 0.7 for most measured parameters, with some of them displaying scores higher than 0.9, indicating that host genetics appears to be a prime factor driving the variation of those parameters (Table 1).

We performed QTL mapping using R/QTL2 (44) to reveal genetic loci associated to the variations in the traits we measured. We identified significant (genome-wide $P < 0.05$; QTL *NK1-3*; Fig. 5, *SI Appendix*, Figs. S7–S9 and Table 2) and suggestive ($P < 0.2$, QTL *NK4-9*; *SI Appendix*, Fig. S10 and Table 2) QTLs that appeared to drive NK cell numbers in the lung (*NK1*) and mLN (*NK4*), the expression level of NKp46 on NK cells from various organs (*NK2*), the frequencies of CD94$^+$ NK cells in the spleen (*NK3*), the

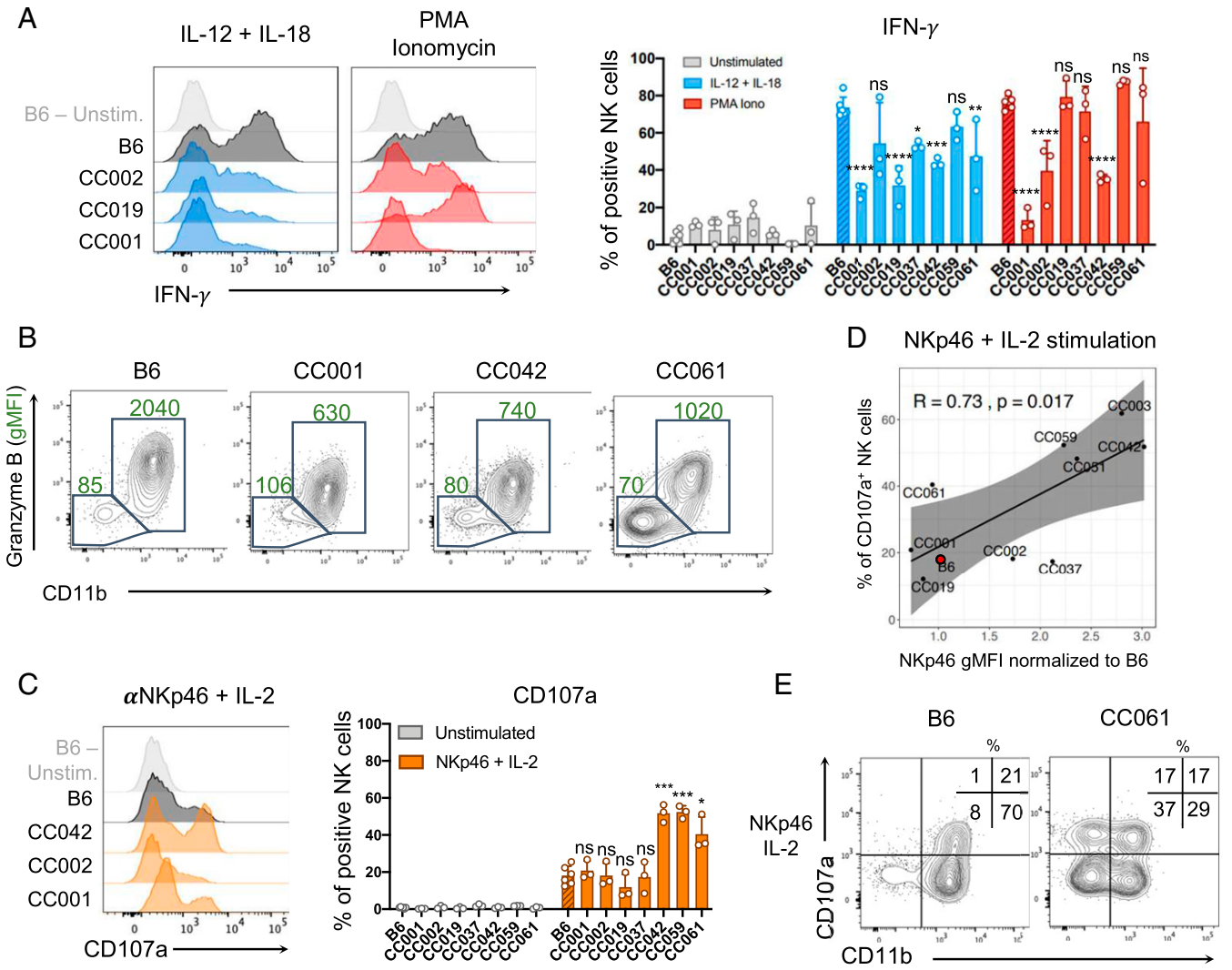

Fig. 4. NK cells from the CC strains present a functional diversity in vitro and in vivo. (*A*, *Left*) Representative histogram overlays of intracellular IFN-γ protein upon IL-12 + IL-18 or PMA + Ionomycin stimulation in splenic NK cells from B6, CC002, CC019, and CC001; (*Right*) bar graph summarizing IFN-γ protein expression by splenic NK cells upon IL-12 + IL-18 or PMA + Ionomycin stimulation in the indicated strains. (*B*) Representative contour plots of Granzyme B versus CD11b expression in splenic NK cells from B6, CC001, CC042, and CC061 following ex vivo IL-2 stimulation. Granzyme B gMFI within each indicated gate appears on the plot. (*C*, *Left*) Representative histograms of CD107a surface expression upon α-NKp46 + IL-2 stimulation by splenic NK cells from B6, CC042, CC002, and CC001; (*Right*) bar graph summarizing CD107a surface expression by splenic NK cells upon α-NKp46 + IL-2 in the indicated strains. For *A* and *C*, a two-way ANOVA was performed followed by multiple comparisons, and each CC line was compared to B6 within each group. (*D*) Correlation graph of the average percentage of CD107a$^+$ NK cells against average NKp46 expression in nine CC strains and B6 (highlighted in red). Regression line, Pearson's R coefficient, and *P* value are indicated. (*E*) Representative contour plots of CD107a versus CD11b expression on splenic NK cells from B6 and CC061 following α-NKp46 + IL-2 stimulation. A two-way ANOVA was performed followed by multiple comparisons between strains. ns = nonsignificant, $*P < 0.05$, $**P < 0.01$, $***P < 0.001$, $****P < 0.0001$.

frequencies of KLRG1$^+$ NK cells in spleen and liver (*NK5*), the frequencies of CD11bSP (*NK6*) and DP cells (*NK7* and *NK8*) in the spleen, and the frequency of DNAM-1$^+$ NK cells in the mLN (*NK9*) (Fig. 5, *SI Appendix*, Figs. S8–S10, and Table 2). We focused on the QTLs that reached genome-wide significance for subsequent candidate gene analysis.

For the number of pulmonary NK cells (Fig. 5*A*), we identified a QTL on chromosome 13, at around 90 Mbp spanning an 8-Mbp support interval (*NK1*; Fig. 5 *B* and *C*). Additional analyses demonstrated that *NK1* was specific to NK cell numbers in the lung but not in other organs. Examination of the founder allele effects split CC strains into two groups: those that inherited the NZO allele at this specific locus harbored significantly more pulmonary NK cells than CC strains that inherited another allele (Fig. 5 *C* and *D* and *SI Appendix*, Fig. S7*A*). We performed a QTL-wide association analysis resulting in 27 genes within *NK1* carrying single nucleotide polymorphisms (SNPs) unique to the NZO background including 16 coding, 8 noncoding, and 3 unclassified genes (Fig. 5*E* and *SI Appendix*, Fig. S7*B*). Only three genes presented nonsynonymous coding variants: *Msh3*, *Xrcc4*, and *Zfyve16* (Fig. 5*E*, Table 2, and *SI Appendix*, Table S2), all of which were of moderate impact according to Variant Effect Predictor analysis (VEP) (45).

QTL mapping analysis of NKp46 expression in hepatic NK cells revealed a QTL at 3.22 Mbp on chromosome 7 with a 3.7-Mbp support interval (*NK2*; *SI Appendix*, Fig. S8 *A* and *B*). *NK2* was associated to NKp46 expression levels from NK cells in other organs as well, which was not surprising given the high correlation of NKp46 expression between organs (Fig. 3*E*). Examination of the founder allele effects revealed that the B6 and WSB alleles

Table 1. Broad-sense heritability scores for the indicated traits

Parameter	Heritability
NK cell numbers	
Spleen	0.67
mLN	0.71
Liver	0.68
Lung	0.67
NK cell differentiation stages: spleen	
% of CD11bSP	0.84
% of $CD11b^+$ $CD27^+$ (DP)	0.59
% of CD27SP	0.90
% of $CD11b^-$ $CD27^-$ (DN)	0.52
Frequencies of $KLRG1^+$ NK cells	
Spleen	0.83
mLN	0.85
Liver	0.87
Lung	0.86
Frequencies of DNAM-1^+ NK cells	
Spleen	0.82
mLN	0.88
Frequencies of $CD94^+$ NK cells	
Spleen	0.93
NKp46 expression levels (NK cells)	
Spleen	0.94
mLN	0.90
Liver	0.95
Lung	0.94
Eomes expression levels (NK cells)	
Spleen	0.71
mLN	0.75
Liver	0.67
Lung	0.75
T-bet expression levels (NK cells)	
Spleen	0.74
mLN	0.62
Liver	0.75
Lung	0.72

were associated with low NKp46 expression levels (*SI Appendix*, Fig. S8 *C–E*). Focusing on genes possessing SNPs unique to the B6 and/or WSB background(s), we identified 14 candidate genes within *NK2* including 10 coding and four noncoding genes (*SI Appendix*, Fig. S8 *F* and *G* and Table S3 and Table 2). None of these genes presented coding variants (*SI Appendix*, Table S3).

Finally, we identified a QTL driving the variation of the frequencies of $CD94^+$ splenic NK cells on chromosome 6 at around 190 Mbp, spanning 9 Mbp (*NK3*; *SI Appendix*, Fig. S9 *A* and *B*). In this case, the founder effects were more complex. At first glance, a large CD94-expressing NK cell population appeared to be correlated with the NZO and A/J alleles (*SI Appendix*, Fig. S9*C*). However, when looking precisely at 133.9 Mbp, we noticed that this high percentage of $CD94^+$ splenic NK cells was not consistent among the CC strains that inherited the A/J allele and that the NZO allele was only present in one CC strain at this locus (*SI Appendix*, Fig. S9*D*). On the contrary, the CAST and WSB alleles were represented in several CC strains at 133.9 Mbp on chromosome 6, and CC strains among these haplotype groups presented more consistent profiles (*SI Appendix*, Fig. S9 *D* and *E*). Both CAST and WSB alleles appeared to negatively influence the percentage of $CD94^+$ NK cells. Among the genes in *NK3*, only 47 genes possessed SNPs specific to the CAST and/or WSB background, of which 36 coding genes and 11 were noncoding genes (*SI Appendix*, Fig. S9 *F* and *G* and Table S4 and Table 2). Only one gene, *Clec2d* encoding Clr-b, presented a nonsynonymous variant (*SI Appendix*, Table S4). Of note, the gene encoding CD94, *Klrd1*, was also among the candidate genes suggesting that variations in the coding or regulatory sequences might influence the frequencies of cells expressing this protein. Comparative analyses revealed more than 98% identity between genomic sequences of *Klrd1* from the eight founder strains (*SI Appendix*, Table S5), yet none of the coding region or promoter polymorphisms could explain the observed variations. Furthermore, none of the identified SNPs fell into one of the 27 open chromatin regions associated with *Klrd1* expression identified in the Immgen Enhancer Networks database (http://rstats.immgen.org/EnhancerControl/index.html). We could identify two SNPs (chr.6: 129,640,167_T/A and chr.6: 129,640,362_G/A) shared by CAST and WSB that represent intronic variants of *Klrc3* coding for the potential CD94 binding partner NKG2E.

Discussion

The CC resource has been conceived and developed by the mouse genetics community to enable a better understanding of how genes control individual trait variation (16). Previous studies estimated that analysis of around 30 CC strains (with on average five mice per strain) would allow uncovering large effect QTLs (46). This suggests that the three significant QTLs we identified—*NK1* (number of NK cells in lung), *NK2* (frequencies of $CD94^+$ splenic NK cells), and *NK3* (expression levels of NKp46 by NK cells from spleen, lung, and liver)—might strongly affect the corresponding NK cell parameter.

Concerning NK cell numbers, we observed large and continuous variations of the values in the different organs across our panel of CC strains. For instance, NK cell numbers in the lung of the two extreme CC strains differed by a factor of 30. These results mirror previous observations made in humans, where 40- to 60-fold differences in lung NK cell frequencies between healthy donors have been reported (15), hereby highlighting the relevance of the CC to model human immune variation. Two of the three genes presenting nonsynonymous variants identified within *NK1*, *Xrcc4* and *Msh3*, encode proteins involved in DNA repair processes, respectively nonhomologous end joining and DNA mismatch repair, and were so far mainly studied for their role in maintaining DNA integrity and preventing cancer onset (47, 48). The third gene, *Zfyve16*, encodes Endofin, an endosomal protein suggested to be involved in the bone morphogenetic proteins (BMP)–Smad signaling pathway through stimulation of Smad phosphorylation (49, 50). Given that in vitro studies of human NK cells suggest that BMPs could play a role in thymic NK differentiation and could favor NK cell function (51, 52), it is conceivable that an Endofin-mediated modification of BMP signaling could affect these processes. However, as VEP analysis indicated that all three nonsynonymous variants appear to only moderately impact gene functions, it is not excluded that other genes within the QTL might influence the absolute numbers of NK cells in the lung. Moreover, given that noncoding RNAs, including microRNAs and long noncoding RNAs, have been shown to exert crucial roles in the regulation of immune cell development and function (53–55), further analyses should consider the impact of polymorphisms in noncoding genes within the QTL as well. The discovery of a genetic factor influencing NK cell homeostasis in a specific microenvironment like the lung would conceivably be of great value for targeted therapies if amenable to therapeutic manipulation.

In this context it is interesting to note that a previous report on adaptive and innate immune cell populations in the spleen, including NK cells identified as $CD3^-DX5^+$ cells, identified two QTLs driving the frequencies of total NK cells and of the $CD27^+CD11b^-$ subset among these total NK cells in the spleen, respectively (20). They reported a negative association of NZO (and NOD) alleles to the frequencies of splenic NK cells yet a positive association of NZO (and WSB) alleles to the frequencies of the $CD27^+CD11b^-$ subset of NK cells in the spleen (20). Collectively, these findings suggest

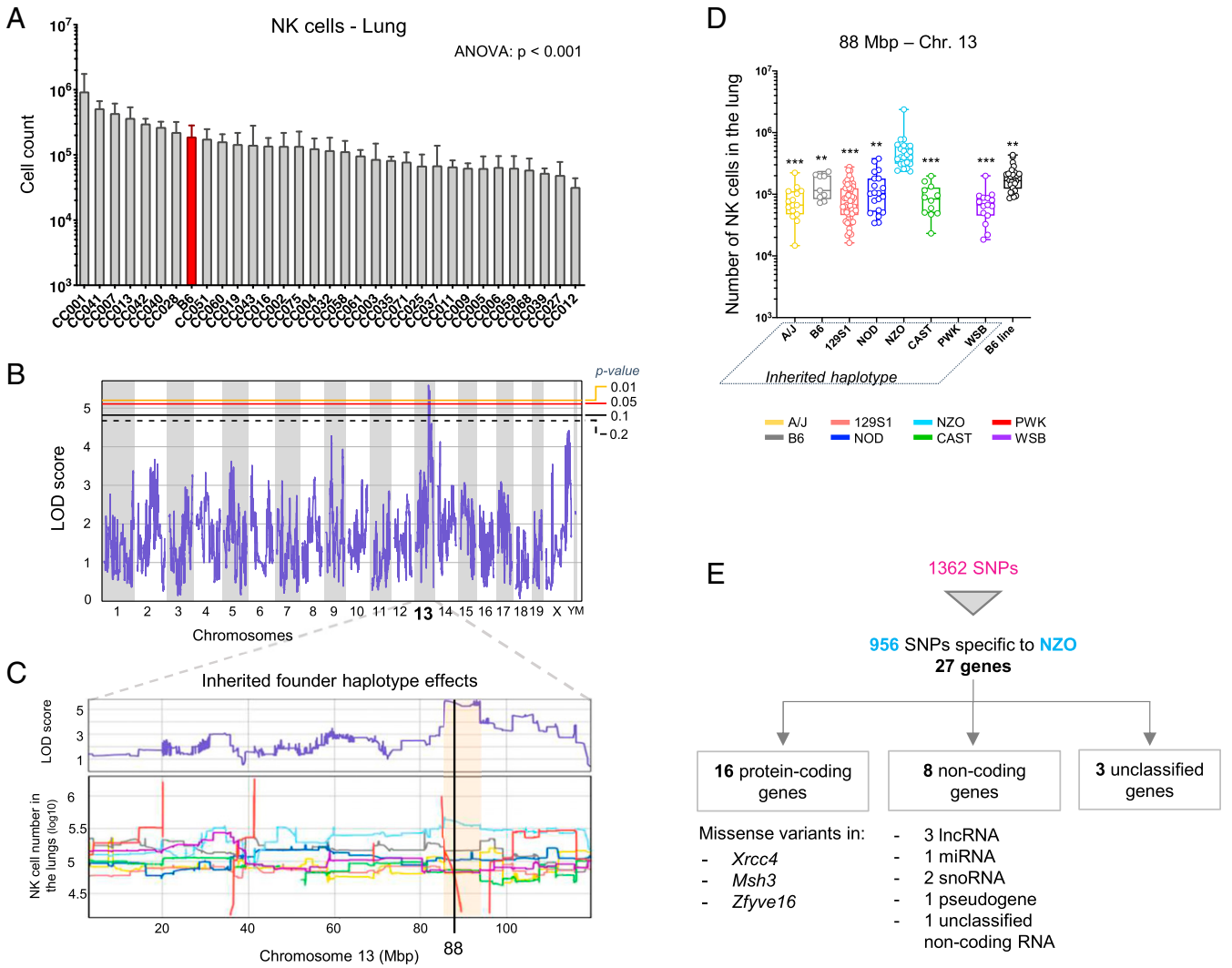

Fig. 5. QTL driving the variation of NK cell number in the lung. (*A*) Number of NK cells in the lung of 32 CC strains and B6. The *P* value corresponds to a one-way ANOVA. Data are represented as mean ± SD (*B*) Genome scan for the number of NK cells in the lung, with a significant peak on chromosome 13 (*P* value thresholds are indicated). Analysis was performed using the qtl2 package in R, and statistical significance thresholds were determined after 10,000 permutations. M: Mitochondria. (*C*, *Top*) LOD score across chromosome 13; (*Bottom*) number of NK cells in the lung depending on the inherited haplotype on chromosome 13. Confidence interval of the QTL is highlighted in orange, and the exact position presented in *D* is represented by the black line. (*D*) Number of NK cells in the lung for each haplotype at 88 Mbp on chromosome 13. A one-way ANOVA was performed followed by multiple comparisons to the NZO group (strains that inherited the NZO allele) with Welch's correction. ns = nonsignificant, $^{**}P < 0.01$, $^{***}P < 0.001$. (*E*) Schematic representation of the strategy used to identify candidate genes and general characteristics of these candidates.

that the NZO genetic background may exert a distinctive but not exclusive influence on NK cell phenotypes.

In contrast to inbred strains such as C57BL/6, 129S1/SvlmJ, and BALB/c (14, 56) that express CD94 at stable frequencies, we observed a large variation of frequencies of $CD94^+$ NK cells in the CC strains (10 to 80%) that matched the variation observed in humans (ranging from 3 to 82%) (12). *NK2*, mapped to chromosome 6, contained only one nonsynonymous variant in *Clec2d* encoding Clr-b. Interactions of Clr-b (or CLEC2D), a broadly expressed C-type lectin-related protein (57), with the inhibitory NK cell receptor NKR-P1B (58) were shown to regulate NK cell functions. However, the frequency of $CD94^+$ NK cells was not affected in *Nkrp1b*$^{-/-}$ mice, suggesting that *Clec2d* may not be involved in the variation of this NK cell trait (58). Interestingly, the list of candidate genes encompassed *Klrd1* encoding CD94. Although the genomic sequences of *Klrd1* were identical at more than 98% among the founder strains, the remaining polymorphisms might explain the observed trait variations. Alternatively, the two intronic variants of *Klrc3* that we identified might influence the prevalence of $CD94^+$ NK cells.

With regard to our analysis of NKp46 expression, we revealed two groups of CC strains: one group expressed NKp46 at levels similar to B6, and the other one expressed two- to threefold higher levels. Such a distribution pattern has not been reported in human cohorts yet, but our experiments suggest that it could influence NK cell responses to NKp46 ligands. *NK3* was mapped to chromosome 7, but none of the 14 genes within this QTL associated to lower NKp46 expression levels presented coding variants. However, two genes, *Tarm1* and *Lair-1*, appeared interesting as they encode inhibitory receptors expressed by subsets of lymphocytes (59–61) including NK cells, suggesting that inhibitory signals might influence NKp46 expression levels. However, further experimentation is required to test this hypothesis.

Table 2. Summary table of identified QTLs related to NK cell parameters

QTL	Phenotype	QTL region	*P* value	Founder effect	Number of SNPs	Number of genes	Top candidate genes
			Significant peaks				
NK1	NK cell number in the lung	Chr. 13: 85.8–93.93 Mbp	0.0077	NZO high	956	27	*Xrcc4*, *Zfyve16*, *Msh3*, *Atg10*
NK2	NKp46 expression in hepatic NK cells	Chr. 7: 3.06–6.75 Mbp	0.0018	B6 and WSB low	226	14	*Lair1*, *Tarm1*
NK3	Frequency of CD94$^+$ splenic NK cells	Chr. 6: 128.22–137 Mbp	0.008	CAST and WSB low	417	47	*Clec2d*, *Etv6*
			Suggestive peaks				
NK4	NK cell number in the mLN	Chr. 4: 102.89–142.91 Mbp	—	—	—	—	—
NK5	Frequency of KLRG1$^+$ NK cells in the liver and spleen	Chr. 19: 3.17–31.23 Mbp	—	—	—	—	—
NK6	Frequency of CD11b$^+$ splenic NK cells	Chr. 7: 36.03–134.99 Mbp	—	—	—	—	—
NK7	Frequency of CD27/CD11b DP	Chr. 10: 88.23–94.47 Mbp	—	—	—	—	—
NK8	splenic NK cells	Chr. 13: 48.18–52.75 Mbp	—	—	—	—	—
NK9	Frequency of DNAM-1$^+$ NK cells in the mLN	Chr. 2: 53.05–76.25 Mbp	—	—	—	—	—

QTLs were considered as significant when $P < 0.05$ and suggestive when $P < 0.2$.

Besides serving as a resource for genetic studies, the CC represents a unique tool to assess the degree of immune variation present and tolerated in *M. musculus* and to discover interdependencies of immune traits. This includes the identification of strains with extreme phenotypes or "outlier" strains that depart from generally conserved correlations. Such strains represent mouse models for the discovery of the molecular mechanisms involved. For example, we observed a range of distributions in CD27- and CD11b-expressing NK cell subsets in different CC lines. The strains CC001 and CC003 represented the extreme ends of this distribution, with the former harboring almost exclusively terminally differentiated CD11bSP cells while immature NK cells predominated in the latter. High scores in heritability analyses indicated that the frequencies of these subpopulations were influenced by genetic elements as suggested by a previous report (20). Accordingly, we identified three suggestive QTLs (*NK6-8*) associated with the prevalence of the different peripheral subpopulations of NK cells including DP and CD11bSP. In addition, a fourth suggestive QTL, *NK5*, was associated with the frequencies of KLRG1$^+$ NK cells. Further exploration of these strains and QTLs might provide novel insights into the mechanisms of NK cell differentiation.

Unexpectedly, NK cell numbers in the liver and/or lung of certain CC strains outnumbered that of tissue T cells. This observation challenges the general concept that innate cell populations are minor compared to predominant adaptive lymphocyte populations. NK cells and T cells have been shown to mutually influence each other during immune responses (62–68). Those studies are mainly based on mouse models using C57BL/6 mice where T cells prevail over NK cells in spleen, liver, and lung, respectively. How corresponding immune responses would unfold in CC mice harboring so different T-to-NK cells ratios remains to be investigated but has the potential to provide new insights into the question of reciprocal regulation of immune cell dynamics and function in health and disease.

The vast variation of immune traits in the CC was also observed with regard to key NK cell functions such as cytokine secretion and degranulation as well. It is important to note that the variation of functional NK cell responses in the CC appeared to mirror the breadth of human NK cell responses to similar stimuli (69, 70). Quantitative as well as qualitative differences in the respective signaling pathways involved could be at the origin of these variations, while the differential expression of NK cell activating and inhibitory receptors, known to dynamically regulate NK cell activity, could also influence some of the observed functional responses of NK cells from the diverse CC strains.

Our observations show that the CC displays ranges of phenotypes rather than discrete, distinct traits, reminiscent of immune phenotypes in large cohorts of healthy individuals (11) and exceeding by far observations made in C57BL/6. While mice are indispensable to explore the role of NK cells in immune responses, the choice of the most adequate mouse model is crucial to enable the extraction of pertinent information and their extrapolation to humans. The restricted allelic diversity of classic mouse inbred strains, which allowed the development of a myriad of transgenic mice and tools to modify the genome with highest precision, ensures limited phenotypic variation. This is advantageous for many experimental approaches; however, it limits their capacity to model the vast phenotypic and functional variation observed in NK cells from healthy human subjects. As discussed above, our results reveal the similarities of NK cell immune variation between human and CC, which is in stark contrast to the lack of thereof in classical inbred strains. This suggests that CC NK cells might be able to phenocopy the variability in responses to interventions observed in humans.

In conclusion, the CC represents a powerful mouse resource for NK cell research. Its extensive genetic and phenotypic diversity can be used to identify candidate genes through genetic mapping analyses or decipher molecular mechanisms leading to outstanding phenotypes, respectively, of relevant NK cell traits. In addition, the CC represents a promising small animal model to test therapeutic strategies targeting NK cells in preclinical settings.

Experimental Procedures

Mice. CC recombinant inbred mice were purchased at the Systems Genetics Core Facility at the University of North Carolina at Chapel Hill or from the Jackson Laboratory and bred in the animal facility of the Institut Pasteur under Specific Pathogen Free (SPF) conditions. In order to ensure a pool of individuals as homogeneous as possible to limit nonheritable variability, we only analyzed female mice of 9 to 11 weeks of age bred in the same SPF animal facility and free of prior involvement in other procedures. We included in each experiment at least one C57BL/6J (B6) mouse serving both as experimental control and reference for antibody staining. For the phenotyping experiments, we analyzed six mice for three strains (CC006, CC037, and CC059), four mice for two strains (CC013 and CC060), two mice for one line (CC039), and five mice for the remaining 26 strains. All mice were randomly allocated to experimental groups. All experiments were approved by the Institut Pasteur Ethics Committee (project dap180067, authorized by the French Ministry of Research in January 2019).

Cell Extraction. Following euthanasia, the spleen and mesenteric mLNs were harvested. Liver and lung were perfused with phosphate-buffered saline (PBS) at room temperature (RT) before resection. Single-cell suspensions from spleens were prepared through mechanical dissociation, while mLNs, livers, and lungs were enzymatically digested using liberase (Roche) and DNase-I (Roche) followed

by density gradient centrifugation using Percoll (GE Healthcare). For more details see *SI Appendix*.

Flow Cytometry Analysis. Cells were stained for viability with Fixable Viability Dye eFluor 506 (eBioscience) in 1X PBS during 15 min on ice. Cells were washed with fluorescence-activated cell sorting (FACS) buffer then stained for extracellular markers in the presence of anti-FcR (anti-CD16/32, clone 2.4G2, Bio X Cell) for 45 min on ice. Following a washing step with FACS buffer, cells were then fixed and permeabilized according to the Foxp3 Transcription Factor Fixation/Permeabilization Kit (eBioscience) protocol. Cells were then intracellularly stained for 30 min at RT with agitation. Antibodies used in this study can be found in *SI Appendix*.

For each CC and each experiment, we calculated the geometric mean fluorescence intensity (gMFI) ratio to B6 of each marker in order to compare expression levels between the CC strains across time.

Data were acquired on a BD LSRFortessa (BD Biosciences) and analyzed with FlowJo software (TreeStar).

In Vitro Cytokine Secretion Assay. For stimulations, 1×10^6 freshly isolated spleen cells were cultured in round-bottom microtiter plates and stimulated for 4 h at 37 °C, 5% CO_2, in RPMI 10% fetal calf serum with the following stimuli: for the degranulation assay, cells were stimulated with immobilized anti-NKp46 (20 μg/mL, clone 29A1.4, BioLegend) with or without addition of IL-2 (10 μg/mL, PeproTech); for detection of IFN-γ, cells were stimulated with IL-12 (1 μg/mL, R&D Systems) or IL-18 (10 μg/mL, R&D Systems) alone or in combination (IL-12 + IL-18) or with PMA (Sigma-Aldrich) and Ionomycin (Sigma-Aldrich); and for detection of Granzyme B, cells were stimulated with IL-2. Anti-CD107a antibodies monensin (GolgiStop, BD Biosciences) together with brefeldin A (GolgiPlug, BD Biosciences) were added at the beginning of the assays. At the end, cells were washed and stained for extracellular markers followed by fixation using BD Cytofix/Cytoperm (BD Biosciences) and finally stained intracellularly with antibodies to Granzyme B, IFN-γ, and Eomes diluted in BD Cytoperm.

Data Normalization. Numerous variables were recorded and were subsequently transformed according to the type of measurement. Number of cells and gMFIs ratios to B6 were log transformed, whereas a logit transformation was applied to percentages prior to performing any univariate or multivariate analyses.

ANOVA and Multiple Comparisons. Comparisons of means among different groups (i.e., strains, treatment, and haplotype groups) were done using one-way or two-way ANOVAs followed by multiple comparisons with Welch's correction or Sidàk's correction. Number of individuals per group is indicated in the Figure legend.

Heritability and QTL Mapping. We consider in this study the so-called "broad-sense" heritability: briefly, it consists in measuring the total variance of a trait and computes the part of this variance that is explained by genetic variations (71).

QTL analysis was performed using R/qtl2 (44) with a mixed effect linear model. The analysis typically consists in three steps: 1) computing the probability of a chromosomal segment to be derived from a given ancestor, based on a hidden Markov model; 2) calculating logarithm of odds (LOD) scores across the genome; and 3) assessing the significance level of LOD scores using ad hoc permutations, as previously published (44). We performed 10,000 permutations for the parameters we analyzed. Our observations being composed of several observations per CC strain, permutations were performed by permuting genotypes across strains to define statistical thresholds and correct multiple testing of the genetic markers. All our statistical corrections were performed in accordance with previously published studies of multiparameter phenotyping of the CC (19, 21, 72, 73).

The SNP databases used for the QTL mapping and candidate gene identification are listed in *SI Appendix*.

Gene Sequence Alignment and VEP Analysis. Gene sequences in FAST-All format from the different CC founder strains were retrieved from the Mouse Genome Informatics database (http://www.informatics.jax.org/genes.shtml) and aligned using basic local alignment search tool for nucleotide sequences (https://blast.ncbi.nlm.nih.gov/Blast.cgi). The impact of SNPs on gene function was assessed using the Ensemble VEP analysis tool. For this, we uploaded the list of SNPs from the identified haplotypes to the VEP-web interface (http://www.ensembl.org/info/docs/tools/vep/index.html), selected the *Ensemble/GENCODE transcripts* database, and run the analyses with default settings without filters and restrictions.

Software. All R-based analyses were performed with R version 3.6.2 in RStudio version 1.3.746. QTL analyses were performed with R/qtl2. Graphical representations were either done with ggplot2 in R or GraphPad Prism. ANOVAs were performed with GraphPad Prism.

Data Availability. All study data are included in the article and/or *SI Appendix*.

ACKNOWLEDGMENTS. We thank Franck Bourgade, Isabelle Lanctin, Pauline Griesmar, Tommy Penel, and Jerôme Le Boydre from the central animal facility of the Institut Pasteur for the care with which they raise the CC mice. We thank Dr. Jean Jaubert, Dr. Neetu Gupta, and all the members of the Innate Immunity Unit for helpful discussions. M.S.J.D. was supported by the French Ministry of Higher Education, Research and Innovation. J.P.D. was supported by grants from the Institut Pasteur, INSERM, and the Ligue Nationale Contre le Cancer (Équipe labélisée Ligue Contre le Cancer).

1. N. Serafini, C. A. J. Vosshenrich, J. P. Di Santo, Transcriptional regulation of innate lymphoid cell fate. *Nat. Rev. Immunol.* **15**, 415–428 (2015).
2. I. Prager, C. Watzl, Mechanisms of natural killer cell-mediated cellular cytotoxicity. *J. Leukoc. Biol.* **105**, 1319–1329 (2019).
3. T. A. Fehniger *et al*., Differential cytokine and chemokine gene expression by human NK cells following activation with IL-18 or IL-15 in combination with IL-12: Implications for the innate immune response. *J. Immunol.* **162**, 4511–4520 (1999).
4. D. H. Raulet, Interplay of natural killer cells and their receptors with the adaptive immune response. *Nat. Immunol.* **5**, 996–1002 (2004).
5. E. Vivier, E. Tomasello, M. Baratin, T. Walzer, S. Ugolini, Functions of natural killer cells. *Nat. Immunol.* **9**, 503–510 (2008).
6. N. D. Huntington, C. A. J. Vosshenrich, J. P. Di Santo, Developmental pathways that generate natural-killer-cell diversity in mice and humans. *Nat. Rev. Immunol.* **7**, 703–714 (2007).
7. K. Kärre, H. G. Ljunggren, G. Piontek, R. Kiessling, Selective rejection of H-2-deficient lymphoma variants suggests alternative immune defence strategy. *Nature* **319**, 675–678 (1986).
8. S. Kim *et al*., Licensing of natural killer cells by host major histocompatibility complex class I molecules. *Nature* **436**, 709–713 (2005).
9. N. C. Fernandez *et al*., A subset of natural killer cells achieves self-tolerance without expressing inhibitory receptors specific for self-MHC molecules. *Blood* **105**, 4416–4423 (2005).
10. J. C. Sun, J. N. Beilke, L. L. Lanier, Adaptive immune features of natural killer cells. *Nature* **457**, 557–561 (2009).
11. E. Patin *et al*.; Milieu Intérieur Consortium, Natural variation in the parameters of innate immune cells is preferentially driven by genetic factors. *Nat. Immunol.* **19**, 302–314 (2018).
12. L. S. Angelo *et al*., Practical NK cell phenotyping and variability in healthy adults. *Immunol. Res.* **62**, 341–356 (2015).
13. A. Gunturi, R. E. Berg, J. Forman, The role of CD94/NKG2 in innate and adaptive immunity. *Immunol. Res.* **30**, 29–34 (2004).
14. M. T. Orr *et al*., Development and function of CD94-deficient natural killer cells. *PLoS One* **5**, e15184 (2010).
15. P. Dogra *et al*., Tissue determinants of human NK cell development, function, and residence. *Cell* **180**, 749–763.e13 (2020).
16. G. A. Churchill *et al*.; Complex Trait Consortium, The Collaborative Cross, a community resource for the genetic analysis of complex traits. *Nat. Genet.* **36**, 1133–1137 (2004).
17. A. Srivastava *et al*., Genomes of the mouse collaborative cross. *Genetics* **206**, 537–556 (2017).
18. T. M. Keane *et al*., Mouse genomic variation and its effect on phenotypes and gene regulation. *Nature* **477**, 289–294 (2011).
19. J. Phillippi *et al*., Using the emerging collaborative cross to probe the immune system. *Genes Immun.* **15**, 38–46 (2014).
20. R. Collin, L. Balmer, G. Morahan, S. Lesage, Common heritable immunological variations revealed in genetically diverse inbred mouse strains of the collaborative cross. *J. Immunol.* **202**, 777–786 (2019).
21. J. B. Graham *et al*., Extensive homeostatic T cell phenotypic variation within the collaborative cross. *Cell Rep.* **21**, 2313–2325 (2017).
22. J. Zhang *et al*., Identification of new loci involved in the host susceptibility to Salmonella Typhimurium in collaborative cross mice. *BMC Genomics* **19**, 303 (2018).
23. R. Green *et al*., Identifying protective host gene expression signatures within the spleen during West Nile virus infection in the collaborative cross model. *Genom. Data* **10**, 114–117 (2016).
24. J. B. Graham *et al*., A mouse model of chronic West Nile virus disease. *PLoS Pathog.* **12**, e1005996 (2016).
25. A. L. Rasmussen *et al*., Host genetic diversity enables Ebola hemorrhagic fever pathogenesis and resistance. *Science* **346**, 987–991 (2014).
26. C. Manet *et al*., Genetic diversity of collaborative cross mice controls viral replication, clinical severity, and brain pathology induced by Zika virus infection, independently of *Oas1b*. *J. Virol.* **94**, e01034-19 (2020).
27. T. Walzer *et al*., Identification, activation, and selective in vivo ablation of mouse NK cells via NKp46. *Proc. Natl. Acad. Sci. U.S.A.* **104**, 3384–3389 (2007).
28. S. M. Gordon *et al*., The transcription factors T-bet and Eomes control key checkpoints of natural killer cell maturation. *Immunity* **36**, 55–67 (2012).
29. M. J. Townsend *et al*., T-bet regulates the terminal maturation and homeostasis of NK and Valpha14i NKT cells. *Immunity* **20**, 477–494 (2004).

30. L. Chiossone *et al.*, Maturation of mouse NK cells is a 4-stage developmental program. *Blood* **113**, 5488–5496 (2009).
31. Y. Hayakawa, M. J. Smyth, CD27 dissects mature NK cells into two subsets with distinct responsiveness and migratory capacity. *J. Immunol.* **176**, 1517–1524 (2006).
32. N. D. Huntington *et al.*, NK cell maturation and peripheral homeostasis is associated with KLRG1 up-regulation. *J. Immunol.* **178**, 4764–4770 (2007).
33. J. M. Wang *et al.*, KLRG1 negatively regulates natural killer cell functions through the Akt pathway in individuals with chronic hepatitis C virus infection. *J. Virol.* **87**, 11626–11636 (2013).
34. B. Müller-Durovic *et al.*, Killer cell lectin-like receptor G1 inhibits NK cell function through activation of adenosine 5′-monophosphate-activated protein kinase. *J. Immunol.* **197**, 2891–2899 (2016).
35. S. H. Robbins *et al.*, Cutting edge: Inhibitory functions of the killer cell lectin-like receptor G1 molecule during the activation of mouse NK cells. *J. Immunol.* **168**, 2585–2589 (2002).
36. J. Yu *et al.*, CD94 defines phenotypically and functionally distinct mouse NK cell subsets. *J. Immunol.* **183**, 4968–4974 (2009).
37. Y. Wang *et al.*, HIV-1-induced cytokines deplete homeostatic innate lymphoid cells and expand TCF7-dependent memory NK cells. *Nat. Immunol.* **21**, 274–286 (2020).
38. K. Van Beneden *et al.*, Expression of Ly49E and CD94/NKG2 on fetal and adult NK cells. *J. Immunol.* **166**, 4302–4311 (2001).
39. M. Salcedo *et al.*, Role of Qa-1(b)-binding receptors in the specificity of developing NK cells. *Eur. J. Immunol.* **30**, 1094–1101 (2000).
40. A. Iguchi-Manaka *et al.*, Accelerated tumor growth in mice deficient in DNAM-1 receptor. *J. Exp. Med.* **205**, 2959–2964 (2008).
41. T. Nabekura *et al.*, Costimulatory molecule DNAM-1 is essential for optimal differentiation of memory natural killer cells during mouse cytomegalovirus infection. *Immunity* **40**, 225–234 (2014).
42. L. Martinet *et al.*, DNAM-1 expression marks an alternative program of NK cell maturation. *Cell Rep.* **11**, 85–97 (2015).
43. A. D. Barrow, C. J. Martin, M. Colonna, The natural cytotoxicity receptors in health and disease. *Front. Immunol.* **10**, 909 (2019).
44. K. W. Broman *et al.*, R/qtl2: Software for mapping quantitative trait loci with high-dimensional data and multiparent populations. *Genetics* **211**, 495–502 (2019).
45. W. McLaren *et al.*, Deriving the consequences of genomic variants with the ensembl API and SNP effect predictor. *Bioinformatics* **26**, 2069–2070 (2010).
46. G. R. Keele, W. L. Crouse, S. N. P. Kelada, W. Valdar, Determinants of QTL mapping power in the realized collaborative cross. *G3 (Bethesda)* **9**, 1707–1727 (2019).
47. S. N. Andres *et al.*, A human XRCC4-XLF complex bridges DNA. *Nucleic Acids Res.* **40**, 1868–1878 (2012).
48. F. Palombo *et al.*, hMutSbeta, a heterodimer of hMSH2 and hMSH3, binds to insertion/deletion loops in DNA. *Curr. Biol.* **6**, 1181–1184 (1996).
49. Y.-G. Chen, Z. Wang, J. Ma, L. Zhang, Z. Lu, Endofin, a FYVE domain protein, interacts with Smad4 and facilitates transforming growth factor-β signaling. *J. Biol. Chem.* **282**, 9688–9695 (2007).
50. J. B. Goh, D. F. Wallace, W. Hong, V. N. Subramaniam, Endofin, a novel BMP-SMAD regulator of the iron-regulatory hormone, hepcidin. *Sci. Rep.* **5**, 13986 (2015).
51. L. Hidalgo *et al.*, Expression of BMPRIA on human thymic NK cell precursors: Role of BMP signaling in intrathymic NK cell development. *Blood* **119**, 1861–1871 (2012).
52. N. C. Robson *et al.*, Optimal effector functions in human natural killer cells rely upon autocrine bone morphogenetic protein signaling. *Cancer Res.* **74**, 5019–5031 (2014).
53. Y. G. Chen, A. T. Satpathy, H. Y. Chang, Gene regulation in the immune system by long noncoding RNAs. *Nat. Immunol.* **18**, 962–972 (2017).
54. A. Mehta, D. Baltimore, MicroRNAs as regulatory elements in immune system logic. *Nat. Rev. Immunol.* **16**, 279–294 (2016).
55. W. K. Mowel *et al.*, Group 1 innate lymphoid cell lineage identity is determined by a cis-regulatory element marked by a long non-coding RNA. *Immunity* **47**, 435–449.e8 (2017).
56. R. E. Vance, A. M. Jamieson, D. Cado, D. H. Raulet, Implications of CD94 deficiency and monoallelic NKG2A expression for natural killer cell development and repertoire formation. *Proc. Natl. Acad. Sci. U.S.A.* **99**, 868–873 (2002).
57. Q. Zhang *et al.*, Mouse Nkrp1-Clr gene cluster sequence and expression analyses reveal conservation of tissue-specific MHC-independent immunosurveillance. *PLoS One* **7**, e50561 (2012).
58. M. M. A. Rahim *et al.*, The mouse NKR-P1B:Clr-b recognition system is a negative regulator of innate immune responses. *Blood* **125**, 2217–2227 (2015).
59. V. Radjabova *et al.*, TARM1 is a novel leukocyte receptor complex-encoded ITAM receptor that costimulates proinflammatory cytokine secretion by macrophages and neutrophils. *J. Immunol.* **195**, 3149–3159 (2015).
60. L. Meyaard *et al.*, LAIR-1, a novel inhibitory receptor expressed on human mononuclear leukocytes. *Immunity* **7**, 283–290 (1997).
61. X. Tang *et al.*, Leukocyte-associated Ig-like receptor-1-deficient mice have an altered immune cell phenotype. *J. Immunol.* **188**, 548–558 (2012).
62. G. Gasteiger *et al.*, IL-2-dependent tuning of NK cell sensitivity for target cells is controlled by regulatory T cells. *J. Exp. Med.* **210**, 1167–1178 (2013).
63. J. Sitrin, A. Ring, K. C. Garcia, C. Benoist, D. Mathis, Regulatory T cells control NK cells in an insulitic lesion by depriving them of IL-2. *J. Exp. Med.* **210**, 1153–1165 (2013).
64. F. Ghiringhelli *et al.*, CD4+CD25+ regulatory T cells inhibit natural killer cell functions in a transforming growth factor-β-dependent manner. *J. Exp. Med.* **202**, 1075–1085 (2005).
65. F. Bihl *et al.*, Primed antigen-specific CD4+ T cells are required for NK cell activation in vivo upon Leishmania major infection. *J. Immunol.* **185**, 2174–2181 (2010).
66. S. N. Waggoner, M. Cornberg, L. K. Selin, R. M. Welsh, Natural killer cells act as rheostats modulating antiviral T cells. *Nature* **481**, 394–398 (2011).
67. P. A. Lang *et al.*, NK cells regulate $CD8^+$ T cell mediated autoimmunity. *Front. Cell. Infect. Microbiol.* **10**, 36 (2020).
68. K. Pallmer *et al.*, NK cells negatively regulate CD8 T cells via natural cytotoxicity receptor (NCR) 1 during LCMV infection. *PLoS Pathog.* **15**, e1007725 (2019).
69. V. Naranbhai *et al.*, Changes in Natural Killer cell activation and function during primary HIV-1 Infection. *PLoS One* **8**, e53251 (2013).
70. C. W. Pohlmeyer *et al.*, Identification of NK cell subpopulations that differentiate HIV-infected subject cohorts with diverse levels of virus control. *J. Virol.* **93**, e01790-18 (2019).
71. W. Kruijer *et al.*, Marker-based estimation of heritability in immortal populations. *Genetics* **199**, 379–398 (2015).
72. M. D. Martin, R. Sompallae, C. S. Winborn, J. T. Harty, V. P. Badovinac, Diverse CD8 T cell responses to viral infection revealed by the collaborative cross. *Cell Rep.* **31**, 107508 (2020).
73. K. E. Noll *et al.*, Complex genetic architecture underlies regulation of influenza-A-virus-specific antibody responses in the collaborative cross. *Cell Rep.* **31**, 107587 (2020).